Materials Today Communications 37 (2023) 106945

Contents lists available at ScienceDirect

Materials Today Communications

journal homepage: www.elsevier.com/locate/mtcomm

Molecular simulation of CO_2 capturing by dual functionalized phosphonium-based amino acid ionic liquids

Kobra Taji, Fatemeh Moosavi *

Department of Chemistry, Faculty of Science, Ferdowsi University of Mashhad, Mashhad 9177948974, Iran

ARTICLE INFO

Keywords:
Amino acid ionic liquid
Carbon dioxide gas capturing
Diffusivity parameter
Molecular dynamics simulation
Tetrabutylphosphonium cation

ABSTRACT

Various solvents have been proposed considering the importance of CO_2 gas removal from the environment. Over the past few decades, ionic liquids (ILs) have elicited much attention due to their unique properties. In this regard, capturing the CO_2 gas by phosphonium-based amino acid ILs (AAILs) was studied by molecular dynamics (MD) simulation. The effect of cation functionalization was studied. The anion was glycinate, $[GLY]^-$, and the cation was tetrabutylphosphonium, $[P_{4444}]^+$, functionalized by different functional groups including acidic (−COOH), alcoholic (−OH), amine ($-NH_2$), and ether ($-OCH_3$). Density, absorption energy, radial distribution function (RDF), mean square displacement (MSD), concentration profile, free volume, and fractional free volume were under investigation. According to density values calculated from MD simulation, functionalized AAIL with a carboxylic acid group ($[P_{4444}COOH][Gly]$) is the most concentrated system with the maximum interaction energy between AAIL and the trapped CO_2 gas equal to − 1.917 $kcal.mol^{-1}$. In addition, the lowest volume variation was observed through this physical absorption. RDF analysis reveals that anion interaction with CO_2 gas is the most considerable one in the case of $[P_{4444}COOH][Gly]$ AAIL. The CO_2 uptake is 2:1 for functionalized AAILs that shows cation functionalization improves CO_2 gas absorption capacity; each mole of $[P_{4444}COOH][Gly]$ AAIL is capable of surrounding 2.11 mol of CO_2. Finally, the gas diffusion coefficient is the lowest one in $[P_{4444}COOH][Gly]$ AAIL as the solvent-free volume is observed as a continuous channel to trap CO_2 gas with the lowest gas diffusivity parameter.

1. Introduction

Greenhouse gases, including water vapor, carbon dioxide, methane, and nitrous oxide, are major contributors to global warming [1,2]. In the atmosphere, carbon dioxide assumes great significance owing to its activity in the infrared domain, its classification as a dangerous greenhouse gas, and the fact that it is one of the most abundant greenhouse gases [3–6]. Given that some of the emitted radiation is reflected by greenhouse gases and doubling the CO_2 concentration increases its emission, the temperature of Earth's surface increases by 0.9 °C [7]. According to Chaban [8], the Earth's average temperature has increased by 0.08 °C/year over the past 12 decades. The main reason for greenhouse gas emissions is human activities that include burning fossil fuels, deforestation, and industrial processes. Production and use of fossil fuel sources such as oil, coal, and natural gas will continue; for this reason, it is necessary to take advantage of effective methods for reducing carbon and other pollutants [9,10]. Numerous materials including metal-organic frameworks, membranes, solid adsorbents, and reactive liquid solvents [2,11], besides the various techniques such as electrochemically-driven separation [12] have been proposed over the past 15 years to improve carbon dioxide gathering. However, capturing the carbon in a source such as coal-fired power plants as a promising way may reduce carbon dioxide [12]. Recently, the utilization of ionic liquids (ILs) due to high dissolution of CO_2 has drawn the attention of many researchers [7, 13–20]. The higher efficiency of the removal process is attributed to their high thermal and chemical stability, as well as low vapor pressure. Following the removal of carbon dioxide, there is a need to reduce the amount of energy for IL regeneration. The adjustable nature and designing new ILs bear great importance because cations and anions form ILs with specific tasks [12, 16, 21–29]. For example, they are applicable in gas solubility. Anthony et al. [30] investigated the solubility of nine different gases in imidazolium-based ILs; they found that carbon dioxide has the highest solubility and the strongest interaction with IL. Hanioka et al. [31] used an especially functional IL to selectively and easily transfer carbon dioxide gas through a membrane. Liquid membranes showed high selectivity and

* Corresponding author.
E-mail address: moosavibaigi@um.ac.ir (F. Moosavi).

https://doi.org/10.1016/j.mtcomm.2023.106945
Received 23 May 2023; Received in revised form 7 August 2023; Accepted 21 August 2023
Available online 23 August 2023

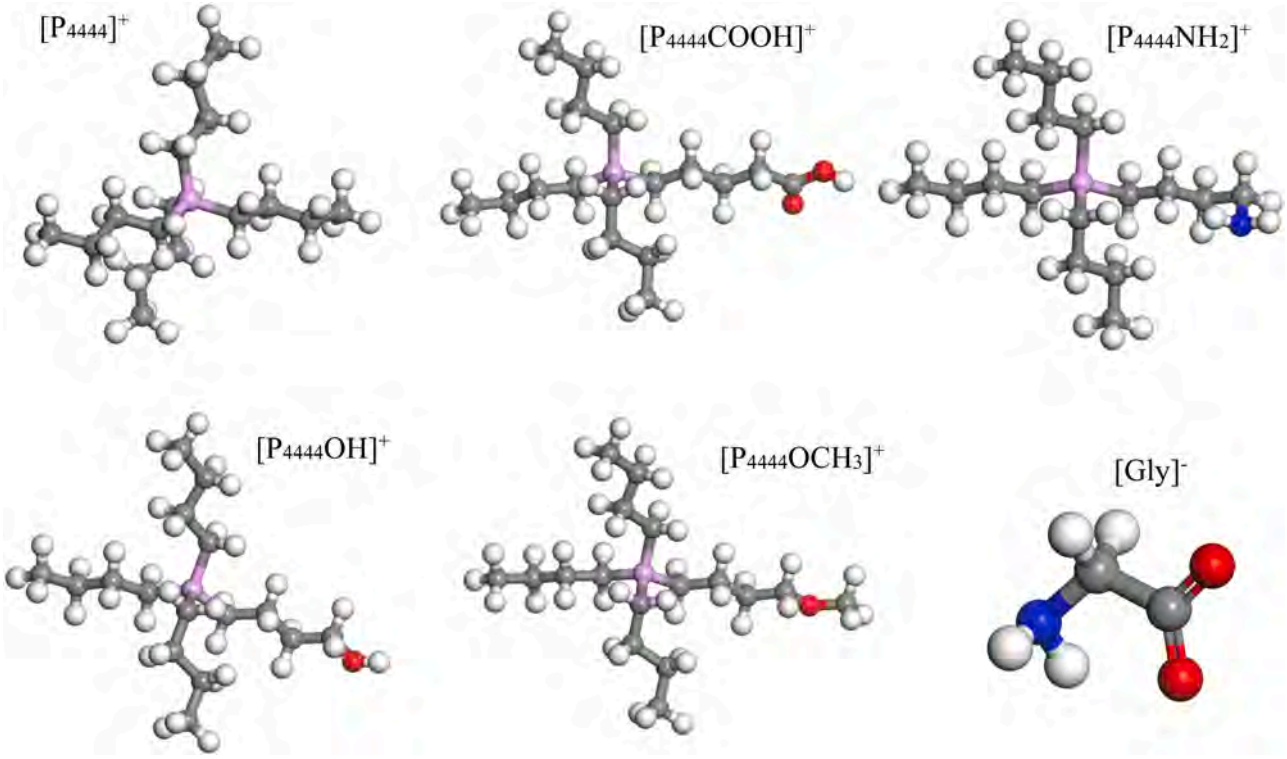

Fig. 1. The structure of cation and anion in the target AAILs. The red color represents the oxygen atom, blue is the nitrogen atom, purple is the phosphorus atom, dark gray stands for the carbon atom, and white is the hydrogen atom.

stability for carbon dioxide separation from gas mixtures. Luo et al. [32] demonstrated that reducing cation…anion interactions in ILs improves CO_2 capturing at 30 °C and 1 atm.

Various cations, including imidazolium, pyridinium, pyrrolidinium, sulfonium, ammonium, and phosphonium are used in IL structure; among these, the phosphonium-based ILs are environmentally friendly and easily accessible. Phosphonium-based ILs have diverse applications due to their structure and physicochemical properties and are adjustable and tunable for specific applications [14,33,34].

Amino acid ionic liquids (AAILs) have potential benefits and applications in gas capturing [13, 35–38]. Functionalized AAILs are a new generation of ILs with a high absorption capacity in the CO_2 capture process. Low viscosity, high resistance to degradation and oxidation, and high biodegradability are the unique properties that make them superior to other ILs [4,28,39]. This class of ILs react with CO_2 and are economically viable due to the use of amino acid raw materials [40]. Noorani et al. [2] synthesized AAILs with 1-butyl-4-methyl pyridinium cation for carbon dioxide absorption and found that the main reason for the higher carbon adsorption capacity in AAILs is the availability of more amine groups. Zhang et al. [41] have synthesized AAILs based on phosphonium cation and observed that the CO_2 uptake capacity is 50% mol. Kasahara et al. [42] have synthesized several phosphonium-based AAILs that can easily transfer carbon dioxide. Among them, phosphonium-based AAIL with proline anion has the best permeability of carbon dioxide and selectivity of carbon dioxide to nitrogen. Not only experimental methods as mentioned above, but also computational chemistry [12, 28, 43–45] and theoretical methods [23,46,47] have been applied to consider the ability of various cations and anions in ILs as well as AAILs for capturing acidic gases, especially CO_2. Shaikh et al. [14] have examined two AAILs $[P_{4444}][Gly]$ and $[P_{1111}][Gly]$ for CO_2 uptake. Free volume and fractional free volume are higher in $[P_{4444}][Gly]$ compared to $[P_{1111}][Gly]$ which promote CO_2 uptake. Tong et al. [13] have performed molecular dynamics (MD) simulations and quantum calculations of 12 AAILs based on phosphonium cation with anions' glycine, proline, imidazole, lysine, and aspartic acid to improve CO_2 uptake. Data analysis from calculations based on density functional theory (DFT) and results of radial distribution function (RDF) indicated the stable adsorption sites of AAILs for CO_2 gas absorption. Li and coworkers [48] have studied the effect of CO_2 gas absorption by trihexyl (tetradecyl)phosphonium imidazolate on IL viscosity change by MD simulation and have found that an asymmetric anion affects the IL viscosity and dynamics.

Kang and coworkers [49] have synthesized dual amino group functionalized imidazolium AAILs and studied the CO_2 absorption mechanism to evaluate cation and anion effects on the AAIL absorbents. Zhang et al. [50] have synthesized AAILs functionalized by amine group and found that (3-aminopropyl)tributylphosphonium aminoethanoic acid salt, $[P_{4444}NH_2][Gly]$, enjoys the largest free volume and thereby the lowest liquid density; as a result, the absorption of CO_2 was 1 mol CO_2 per mol IL, which is also true in the case of tetrabutylammonium glycinate ($[N_{4444}][GLY]$) [51]. According to these studies, here, bio-renewable AAILs with non-toxic [52] and more thermal stable alkyl chains were selected because of their appreciated ability for gas absorption and lubrication [13,53]; the AAIL's cation is tetrabutylphosphonium ($[P_{4444}]^+$) and glycinate anion ($[Gly]^-$). The cation of AAILs was functionalized and studied by different functional groups. RDF, coordination number, concentration profile, mean square displacement (MSD), free volume, and fractional free volume are investigated. In fact, by examining these properties, the effect of adding a functional group into the cation is investigated for CO_2 absorption. The foundation for such simulations is a molecular understanding of CO_2 physical absorption by these AAILs to explore the effect of the functional group of the cation alkyl chain on the gas capturing. Though many researchers have studied the absorption of acid gases both experimentally and theoretically, as mentioned above, the gas absorption by AAILs is still obscure. Consequently, various structural factors affecting the absorption of CO_2 are discussed based on the present results.

Table 1
A summary of the computational studies on phosphonium-based ILs.

Cation name	Anion name	Level of computation	Force field	Software	Ref.
methoxy(triethyl(methoxymethyl)phosphonium and triethyl(2-methoxyethyl)phosphonium	bis(trifluoromethylsulfonyl)imide	B3LYP/6–31 +G(d)	AMBER	AIQM: Gaussian MD: M.DynaMix	[65]
trihexyl(tetradecyl)phosphonium	bis(trifluoromethylsulfonyl)imide	B3LYP/6–31 +G(d)	AMBER	AIQM: Gaussian MD: MDynaMix	[68]
tetrabutylphosphonium	trifluoroacetate, acetate, and hexafluorophosphate	B3LYP/6–31 +G*	AMBER	AIQM: Gaussian MD: GROMACS	[69]
tetrabutylphosphonium	2-cyanopyrrolide	B3LYP/ 6–311 + +G* *	-	AIQM: GAMESS	[8]
tetrabutylphosphonium	glycine, alanine, serine, lysine, leucine, isoleucine, phenylalanine, proline, methionine, aspartic acid, glutamic acid, glutamine, and taurine	B3LYP/ 6–311 +G* *	AMBER	AIQM: Gaussian MD: M.DynaMix	[70]
tributyl(2-ethylhexyl)phosphonium, trioctyl(2-ethylhexyl)phosphonium, and trioctyl(undecyl) phosphonium	bromide	B3LYP/6–31 G(d,p)	-	AIQM: Gaussian	[71]
tetrabutylphosphonium	4-(methoxycarbonyl)phenol	B3LYP-D3BJ/ 6–311 + +G(d,p)	-	AIQM: VASP	[72]
trihexyl(tetradecyl)phosphonium	chloride and bistrifluoro(sulfonyl)imide	B3LYP/ 6–311 + +G* *	-	AIQM: Gaussian	[73]
trihexyl(tetradecyl)phosphonium	lysine	B3LYP/6–31 + G*	-	AIQM: Gaussian	[74]
tetraalkylphosphonium, tributyl(octyl)phosphonium, tributyl(tetradecyl)phosphonium, and trihexyl (tetradecyl)phosphonium	bis(mandelato)borat, bis(malonato)borate, bis(oxalato) borate, and bis(salicylato)borate	B3LYP/ 6–311 + +G(d)	AMBER	AIQM: Gaussian MD: M.Dynamix	[75]
trihexyl(tetradecyl)phosphonium	prolinate and methioninate	B3LYP/ 6–311 G+ +(d,p)	-	AIQM: Gaussian	[76]
tetraethylphosphonium	phenolate, 4-nitrophenolate, and 4-methoxyphenolate	B3LYP/6–311 +G (d,p)		AIQM: Gaussian MD: CPMD	[77]
n-alkylpyridinium	chloride, bromide, and dicyanamide	RHF/6–31 G(d)	OPLS-AA	AIQM: Gaussian MD: DL_POLY	[78]

2. Simulation details

Every simulation was performed at a temperature of 298 K and a pressure of 1.01325×10^5 Pa, equivalent to 1 atm. The structure of each ion pair of AAIL was first optimized by quantum computing at the computational level of B3LYP/6–311 + +G(d,p); after ensuring the stable structure and minimum energy, the partial atomic charges were computed at the same computational level by the CHELPG method using Gaussian09 [54]. The resulting structure containing the calculated atomic partial charges was entered into Materials Studio software version 2017 [55,56] to perform molecular dynamics simulation. Moreover, a simulation cell with a density of 1.00 $g.cm^{-3}$ containing 50 pairs of ions was prepared from AAILs at ambient temperature and the force field for this system was selected COMPASS [57,58]. Energy minimization and geometric optimization of each simulation cell were continued up to the energy convergence tolerance equal to 2×10^{-5} $kcal.mol^{-1}$, the displacement was 1×10^{-5} Å, and the force was equal to 0.001 $kcal.mol^{-1}.Å^{-1}$. Therefore, the simulation cell was ready to perform the MD simulation in an isothermal-isobaric ensemble, NPT, at the target temperature and pressure. The Maxwell-Boltzmann velocity distribution at 298 K was used to establish the random velocity of each atom at the beginning of the simulation. The velocity Verlet integration algorithm, the Andersen thermostat [59] for controlling the temperature, the Berendsen barostat for the pressure [60], and 1000,000 steps with a time step of 1 fs were applied for all simulations. After 1 ns of the simulation, it was ensured that the system has found its correct density; the energy, temperature, pressure, and volume of the simulation cell are fixed; as a result, the simulations were performed for one another nanosecond (1 ns) in canonical ensemble with constant particle number, volume, and temperature (NVT). To collect data and perform analyses for the results of the simulation and remove the effects of external constraints (thermostat and barostat), the simulation was continued in an isolated simulation cell, microcanonical ensemble (NVE), with the number of particles, volume, and energy being constant for another 1 ns. Long-range corrections were made at all stages of atomic simulation; the cut-off radius of non-bonding interactions was 15.5 Å. For modeling electrostatic interactions, the Ewald summation method with an accuracy of 0.0001 $kcal.mol^{-1}$ was used. In this study, the effect of functional groups including carboxylic acid, −COOH, hydroxyl, −OH, methoxy, $-OCH_3$, and amine, $-NH_2$, on the alkyl chain of phosphonium cation was under investigation; each one is symbolized by $[P_{4444}COOH][Gly]$, $[P_{4444}OH][Gly]$, $[P_{4444}OCH3][Gly]$, and $[P_{4444}NH_2][Gly]$, respectively. Noticeably, the functional group was added to the end of one of the butyl chains of cation. The structure of cations and anion of AAILs studied here are illustrated in Fig. 1.

All the above steps were repeated to simulate the mixed system (system containing 50 ion pairs of AAIL and 10 molecules of CO_2). First, the gas was optimized at the same level of theory applied for AAILs, the atomic charges were computed by the CHELPG method at B3LYP/6–311 + +G(d,p) level of theory, and then the gas molecules were randomly positioned in the simulation cell. The same procedure of the pure AAIL system was applied in the MD section by performing a 3 ns MD simulation to let the gas be distributed between AAIL ion pairs.

To be sure that the density of each bulk system has converged to the real value at the temperature and pressure under study, the NPT ensemble was applied. Then, the volume was considered to be constant to control the temperature of the system; this step was performed in NVT ensemble. If the system is in the stationary state with the temperature and density constant at mild conditions, all forces are removed and the system is considered to be isolated, i.e., NVE ensemble. The same procedure has been applied previously by other researchers [61–67]. The corresponding simulation time was selected based on the lowest fluctuation in properties such as density, temperature, and potential energy. The following figures show the trend of these properties in simulation through the last 1 ns of MD simulation.

According to the literature [8, 65, 68–77], it can be found that the most widely used ab initio quantum mechanical (AIQM) approach to find the stationary state of an ion pair is DFT that utilizes the Becke's three-parameter with Vosko et al.'s local correlation part, abbreviated as B3LYP. To make it more understandable a summary of the phosphonium-based ILs selected and the methods applied are given in Table 1.

From the other side of view, among the non-polarizable, non-reactive force fields, the AMBER force field parameter sets have been developed

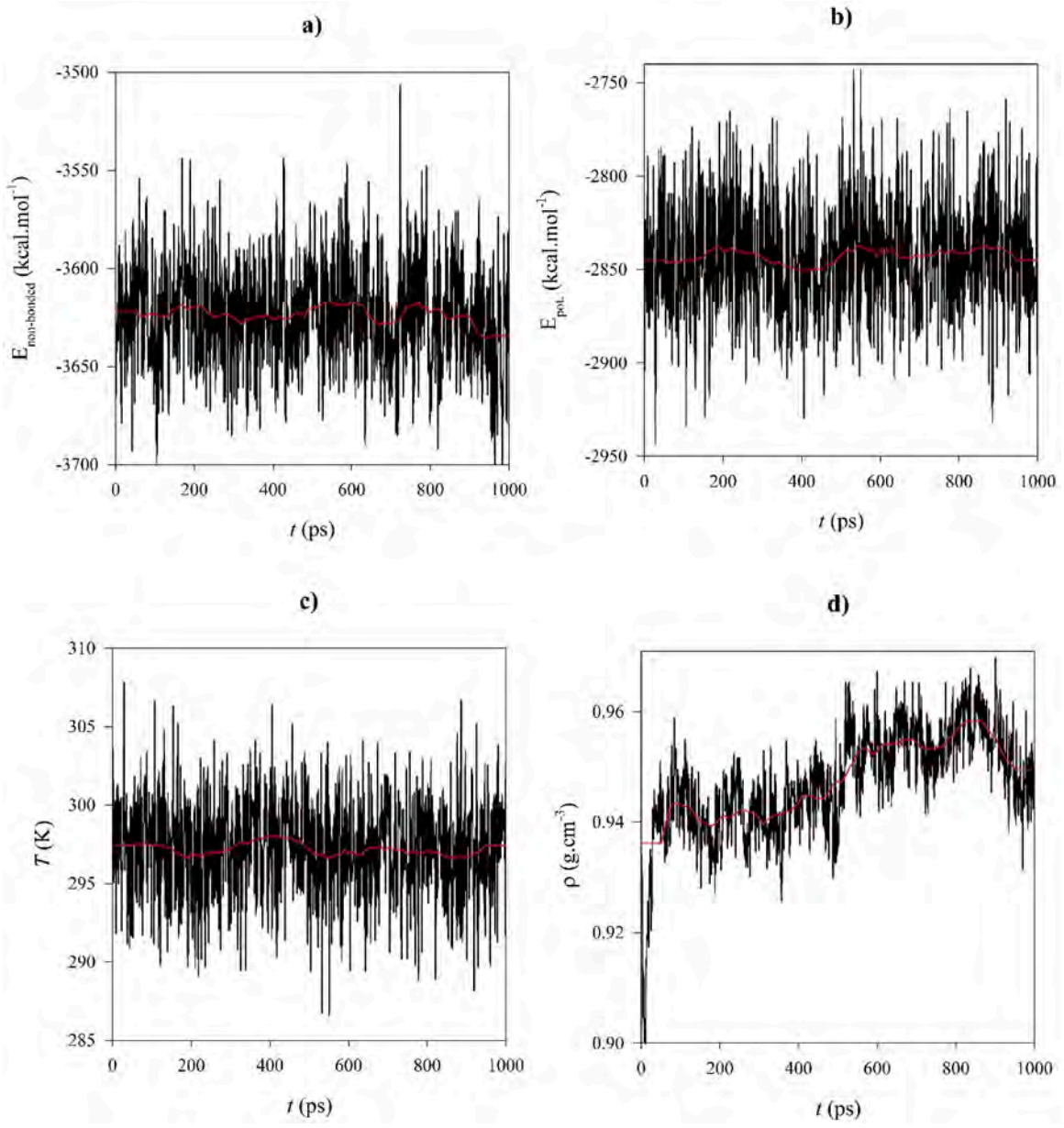

Fig. 2. The instance (black line) and average variation (red line) of a) $E_{\text{non-bonded}}$, b) $E_{\text{pot.}}$, c) T, and d) ρ with simulation time for $[P_{4444}][Gly]$ at last 1 ns of simulation.

for the widest range of phosphonium ILs cation-anion pairs. COMPASS that stands for Condensed-phase Optimized Molecular Potentials for Atomistic Simulation Studies is the force field of choice underlying materials science applications of the BIOVIA brand as well as supporting many classical applications within Materials Studio. Considering these references, it is highlighted that the selected AIQM has great effect on the ion pair structure that is applied as an initial configuration for MD. In addition, whatever force field is more accurate, the results of MD simulation are in accurate agreement with the experiment. As an instance, the deviation error for computed density of $[P_{4444}][Gly]$ at ambient conditions is lower than results reported by Liu et al. [65]; the current results can be validated. Liu et al. [65] have shown that the error in predicting density is greater than 5% in the case of $[P_{2,2,2,1O1}][Tf_2N]$ and $[P_{2,2,2,2O1}][Tf_2N]$.

It should be notified that the current study was performed at a single temperature and pressure since the effect of temperature and gas pressure on absorption process are not the main points here. Furthermore, as previous studies [32,72,76,77,79,80] have performed at ambient and normal temperature and pressure, the current study has also performed the same. The most important point is that it is important to capture pollutant gases at not harsh conditions.

Another doubt that is come to the mind is that the procedure for adding the CO_2 molecules is arbitrary; consequently, the effect of the CO_2 molecules starting location of the gas as well as the simulation time are needed to be under study. Outstandingly, the initial locations of the CO_2 gas molecules do not play a critical role in macroscopic properties that are independent of the structure and atomic position. In addition, if the system has converged from the structure point of view, the atoms have found their stable positions and the coordination numbers will not change by another longer time simulation. As a result, the absorption energy, absorption capacitance, and density will be constant if someone continues the simulation or changes the initial location of the CO_2 molecules. The same observation has been checked previously for simulation time [81].

Table 2
Density, absorption energy, and volume variation concerning the pure state in the systems containing gas and AAIL studied at 298 K.

AAIL	ρ (g.cm^{-3})	$E_{abs.}$ (kcal.mol^{-1})	ΔV (Å^3)
[P_{4444}][Gly]	0.959	-1.704	537.135
[$P_{4444}NH_2$][Gly]	0.997	-1.785	664.001
[P_{4444}COOH][Gly]	1.041	-1.917	206.977
[P_{4444}OH][Gly]	1.018	-1.834	331.507
[$P_{4444}OCH_3$][Gly]	0.989	-1.751	888.242

3. Results and discussion

To be sure the equilibration has occurred, the variation of non-bonded energy, potential energy, temperature, and density with simulation time was under consideration. See Fig. 2 for more details.

According to Fig. 2, it can be received that the fluctuations are around average values of ρ, T, $E_{\text{non-bonded}}$, and $E_{\text{pot.}}$. As the fluctuation is lower than $\sqrt{N^{-1}}$ [81], the simulation time can be acceptable. It is shown that the $E_{\text{pot.}}$ fluctuation is less and the relative error between the average values and instantaneous values are less than 0.03 and temperature fluctuates around 298 K with a not considerable variance. Besides the selection of initial structures taken from an accurate AIQM

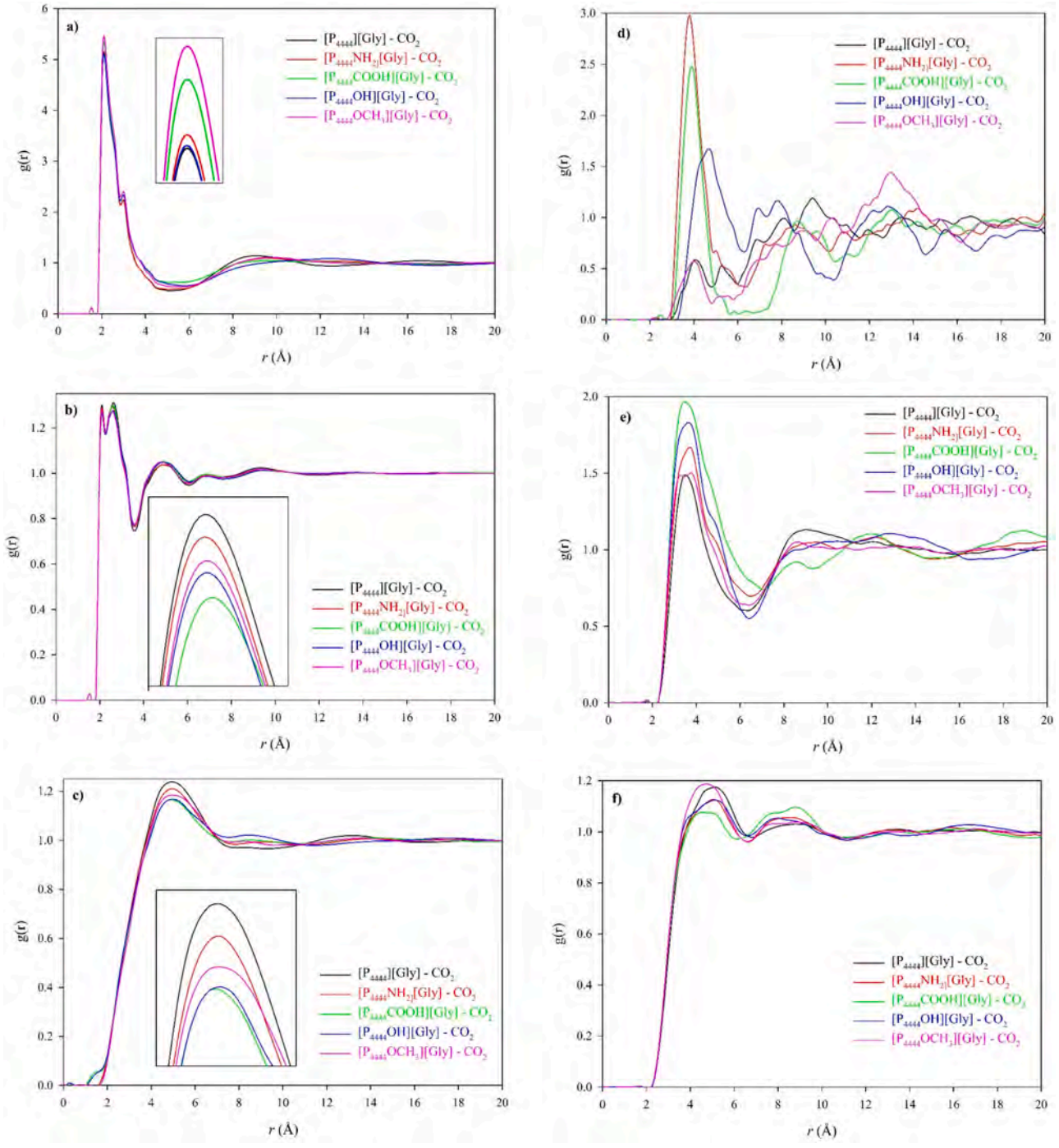

Fig. 3. Different RDFs for the system containing AAIL and CO_2 gas at 298 K a) anion-anion, b) cation-cation, c) cation-anion, d) CO_2-CO_2, e) CO_2-anion, and f) CO_2-cation. The indented part in a), b), and c) corresponds to the magnified first peak of RDF.

Table 3
CN values for simulated systems at 298 K.

AAIL	Anion-CO_2	CO_2-CO_2	Cation-Anion
[P_{4444}][Gly]	1.52	0.24	3.55
[$P_{4444}NH_2$][Gly]	1.81	1.60	3.50
[P_{4444}COOH][Gly]	2.11	0.94	3.07
[P_{4444}OH][Gly]	1.90	1.64	3.28
[$P_{4444}OCH_3$][Gly]	1.58	0.22	3.08

method, the accuracy in computing the atomic charges, and the small deviations in molar densities in comparison to experiment shed light on the consistencies in the simulations.

The thermophysical properties such density values of the AAILs at 298 K and 1 atm were calculated. The density of studied pure non-functionalized AAIL ([P_{4444}][Gly]) is 0.952 g.cm^{-3} that is in excellent agreement with the corresponding experimental value, 0.960 g.cm^{-3} [13] and confirms that carefully chosen conditions are acceptable. In addition, Zhou et al. [70] have simulated AAILs based on amino acid anion by AMBER force field at the same temperature and pressure, the density calculated is 0.954 g.cm^{-3}. ReaxFF has been applied by Zhang et al. [79] and the density value is 0.976 g.cm^{-3} at 300 K which is greater than its corresponding experimental value. Generalized AMBER force field (GAFF) has been applied to find the density of [P_{4444}][Gly] AAIL [14]; it was found that at 300 K the density is equal to 0.993 g.cm^{-3}. All these results reveal that the current simulation is in excellent agreement with the experimental and theoretical density values. In the case of mixture systems containing 50 AAILs and 10 CO_2 gas molecules, the density values are reported in Table 2. Zhang et al. [79] have reported a density of 1.000 g.cm^{-3} in the case of a 16.7 mol% mixture of CO_2 and [P_{4444}][Gly] AAIL that agrees well with increasing the density due to the absorbed gas interaction with this AAIL.

According to the table, [P_{4444}COOH][Gly] AAIL experiences the highest density corresponding to the most concentrated system, the highest gas absorption energy per each ion pair of AAIL $\left(E_{abs} = \frac{E_{AAIL+CO_2} - E_{AAIL}}{N_{AAIL}}\right)$, and the lowest volume variation $(\Delta V = V_{AAIL+CO_2} - V_{AAIL})$ due to the gas absorption. Computing the system volume before and after absorption can be a metric to differentiate target AAILs in their ability of absorb CO_2 gas since is a sign of gas distribution in the simulation box. These results can shed light on [P_{4444}COOH][Gly] ability to enjoy the strongest interaction with captured gas. It is worth to mention that E values in $E_{abs.}$ are total intermolecular energies including van der Waals energy and electrostatic terms. The results demonstrate that cation functionalization by electron-withdrawing functional groups improves the gas capturing by AAIL. To explore a molecular deep insight into the system and to investigate the molecular behavior of each AAIL, the RDFs between the center of mass of cation, anion, and CO_2 gas were evaluated and analyzed for the mixed system containing AAIL and carbon dioxide gas. Fig. 3 displays the different pair correlation functions between the species of the system containing cation, anion, and captured CO_2 gas.

Among all the pair correlations, the interaction of anions with each other is the strongest because of the hydrogen bond between anions; in addition, according to the figure, anion plays the main role in gas absorption. The interaction between all species is affected by the cation functional group and is the lowest in the case of non-functionalized AAIL while is the strongest in the case of [$P_{4444}OCH_3$][Gly] AAIL. It seems that the bulkiness of the functional group has a direct relationship with the strength of the interaction between the anions. The position of the peaks shows that adding a functional group to the cation does not change the interaction position of the anions although the anion-anion interaction experiences a change in strength. In the case of cation-cation interaction, Fig. 3b, the peak location is at 2.60 Å which is 0.4 Å away from the anion-anion interaction location. Moreover, the pair correlation contains two branched peaks followed by a short and wide one. The presence of the second coordination layer in the RDF between cations confirms that there is no aggregation of the cations due to their large size and relatively symmetrical structure of the cation. This lack of accumulation can indicate the orientation of cations. The intensity order of RDF peaks does not variate significantly with the alteration of the functional group and interactions are weakened by the addition of a functional group. The weakest cation-cation interaction is observed in the case of [P_{4444}COOH][Gly] AAIL. Considering cation-anion interaction, Fig. 3c, it can be found that non-functionalized AAIL, [P_{4444}][Gly], enjoys the strongest cation-anion interaction while the same one is the most insignificant in the case of [P_{4444}COOH][Gly]. In summary, the interaction of anions with each other is stronger than cations with each other and cations with anions. Based on Fig. 3d, due to the greater movement of gas molecules and their irregular movement, the RDF dependency on position experiences more fluctuations. The presence of the second and third peaks in the structural analysis confirms that the gas molecules are scattered inside the simulation cell. The interaction of carbon dioxide gases with each other in the AAIL containing the amine functional group ([$P_{4444}NH_2$][Gly]) is the strongest and in the case of [P_{4444}OH][Gly] is the weakest. The position and intensity of the CO_2-CO_2 RDF peaks show that [P_{4444}COOH][Gly] AAIL can perfectly dissolve the gas molecules as a green liquid solvent. From the other side of view, the difference between the first and second layers of CO_2 trapped molecules into [P_{4444}COOH][Gly] AAIL, in which molecules interact as pairs and quad molecules, is approximately 4 Å while in the case of [$P_{4444}NH_2$][Gly], one sharp and narrow peak exists. This observation confirms that CO_2 gas molecules do not accumulate and physically interact with each other; therefore, these all studied AAILs can dissolve this gas to some extent. According to Fig. 3e, the strength of interactions between gas and anion follows [P_{4444}COOH][Gly] > [P_{4444}OH][Gly] > [$P_{4444}NH_2$][Gly] > [$P_{4444}OCH_3$][Gly] > [P_{4444}][Gly] trend; the average distance between anion and CO_2 gas is 3.44 Å and this value between CO_2 gases is 3.80 Å that indicates a closer distance between anion and CO_2 gas compared to the CO_2 gas molecules. Therefore, [P_{4444}COOH][Gly] AAIL has the highest ability to absorb CO_2 gas which is also in accordance with the cation-anion pair correlation function. As [P_{4444}][Gly] has the strongest interaction between cation and anion, its tendency towards CO_2 gas is the most ignorable. Therefore, due to the weak interaction between the cation and the anion, [P_{4444}COOH][Gly] AAIL has the greatest ability to absorb CO_2 gas, e.g., a strong interaction between anion and CO_2 gas is observed. Based on Fig. 3f, the RDF between CO_2 gas and the center of mass of the cation observes insignificant intensity as well as being at a further distance. The closest distance between cation and CO_2 gas is larger than 4 Å; consequently, the interaction between the gas and cation is insignificant compared to an anion and captured gas. It can be concluded that the anion-CO_2 strength is greater than the cation-CO_2 interaction, i.e., AAIL functions by its anion to carry out gas absorption.

To determine the solubility of CO_2 gas in each AAIL, the number of gases around cations and anions should be compared with the number of cations and anions placed next to each other and the CO_2 gases. According to the RDF and the closest distance between each pair, the position of the first peak (r_{min}), the coordination number (*CN*) can be calculated:

$$CN = 4\pi \quad \rho \int_0^{r_{min}} r^2 g(r) dr \tag{1}$$

The *CN* values of anion-cation, anion-CO_2, and gas-gas were investigated and are reported in Table 3.

The number of anions around the cations is greatest in the case of [P_{4444}][Gly] AAIL with a value of about 4 while [P_{4444}COOH][Gly] AAIL involves 3 cations around each anion that demonstrates [P_{4444}][Gly] AAIL is not enthusiastic about gas dissolution and the lowest anion-gas CN accompanies this fact. The strongest absorption ability in [P_{4444}COOH][Gly] AAIL can be related to its highest CN between anion and CO_2 gas. As the cation-anion interaction is weaker if AAIL is

Table 4
AIQM results computed at B3LYP/6–311 + +g(d,p) level of theory for AAILs.

AAIL	E_g (eV)	χ (a.u.)	η (a.u.)	Electrophilicity (a.u.)	E2 (kcal. mol^{-1})
$[P_{4444}][Gly]$	4.0872	0.1094	0.0751	0.0797	8.960
$[P_{4444}COOH]$ [Gly]	4.0706	0.1082	0.0748	0.0783	8.250
$[P_{4444}OCH_3]$ [Gly]	4.1587	0.1099	0.0764	0.0790	8.990
$[P_{4444}OH]$ [Gly]	4.0888	0.1086	0.0751	0.0785	8.250
$[P_{4444}NH_2]$ [Gly]	4.0259	0.1071	0.0740	0.0776	5.240

functionalized, the more space can be provided between cation and anion; consequently, adding a functional group to the cation alkyl chain causes more gases to be surrounded by AAIL. Due to the presence of 2 CO_2 gas molecules around each anion of AAIL, it can be expressed that the solubility of CO_2 gas in these AAILs is 1:2, e.g., two molecules of CO_2 gas are dissolved by each ion pair. Zhang et al. [41] have also applied AAILs based on phosphonium cation and the same ratio of gas absorption to AAIL was found if there is no water present in the system. However, the crucial point of the present study is that cation functionality, though the cation has the second role in gas absorption by AAIL, enhances solvent ability in gas dissolution and the maximum CO_2/AAIL ratio is achieved. In other words, cation functionalization improves CO_2 gas absorption by AAIL. This difference in gas absorption through cation functionalization is in accordance with the difference in the local structure and its effect on different CO_2 absorption mechanisms [80].

Interestingly, the AIQM results including HOMO-LUMO gap (E_g), electronegativity (χ), hardness (η), and second order perturbation energy (E2) between cation and anion computed at B3LYP/6–311 + +g(d, p) level of theory show the highest values for $[P_{4444}OCH_3][Gly]$ AAIL that related to its stability and reactivity. In addition, the mentioned AAIL has the lowest electrical chemical potential ($\mu = -\chi$) in accordance to the other target AAILs. Table 4 outlines these AIQM characteristics for all studied AAILs. However, the values of electrophilicity do not show any correlation.

The next question is how the absorbed gases are distributed in a special direction, such as the *x* direction. To have a look at cation, anion, and CO_2 gas distribution, the relative concentration profile is examined; see Fig. 4 for more details.

According to the cation concentration profile, Fig. 4a, $[P_{4444}][Gly]$ AAIL has three broad and long peaks with the same changes and two

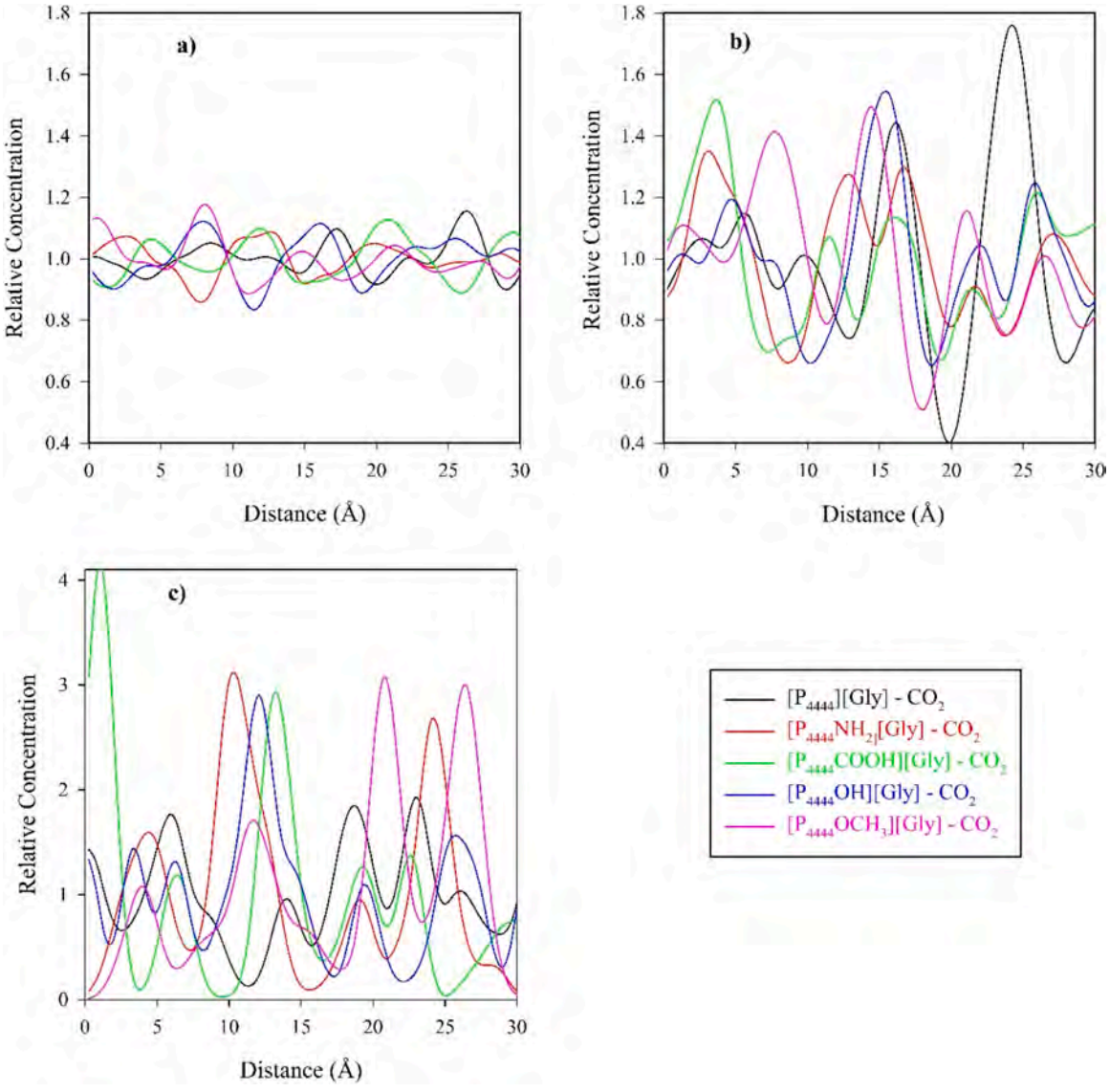

Fig. 4. Concentration profile of a) cation, b) anion, and c) CO_2 concerning *x* direction at 298 K.

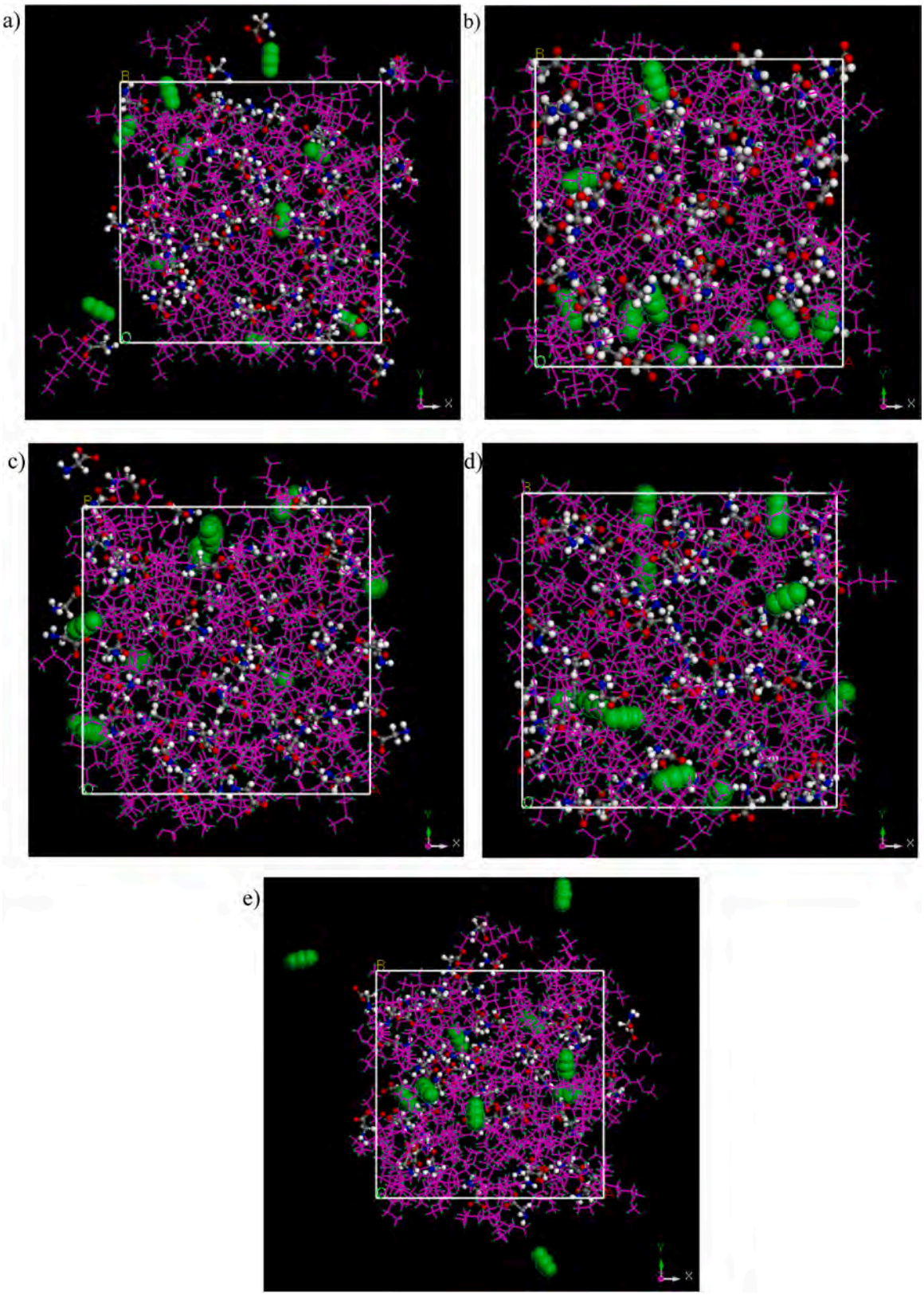

Fig. 5. Graphical representation of simulation cell; a) [P_{4444}][Gly] AAIL, b) [$P_{4444}NH_2$][Gly] AAIL, c) [P_{4444}COOH][Gly] AAIL, d) [P_{4444}OH][Gly] AAIL, and e) [$P_{4444}OCH_3$][Gly] AAIL. Gas atoms are shown as green spheres, cations are shown as lines, and anions are shown as CPK, i.e., ball and stick.

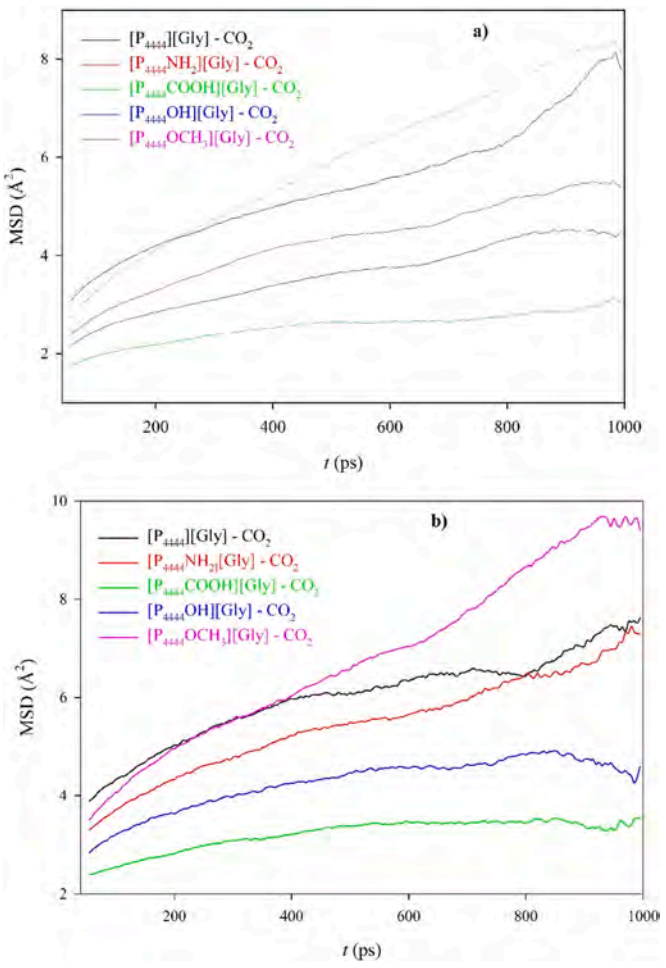

Fig. 6. Time dependence of MSD at the final 1 ns of simulation at 298 K a) anion and b) cation.

shorter peaks while these are converted to three broad peaks in $[P_{4444}COOH][Gly]$ AAIL. The peaks are not located at a fixed distance from each other, i.e., the cations do not have the same distribution and are located at different distances from each other in the *x* direction. Therefore, it can be said that due to the presence of CO_2 gas as well as the functional group, cation profile concentration in the *x* direction changes and follows a non-uniform trend in cases where there is the most interaction between the gas and the AAIL. In the case of $[P_{4444}][Gly]$ AAIL, one long and wide peak besides three short peaks are observed if the anion concentration profile is under consideration. Fig. 4b shows that the anions enjoy a higher concentration and follow a non-uniform distribution in the *x* direction because the peaks are not at the same distance from each other. Therefore, $[P_{4444}][Gly]$ AAIL witnesses a non-uniform distribution of anions in a specific direction, e.g., the *x* direction. The anion concentration profile of $[P_{4444}COOH][Gly]$ AAIL demonstrates the least fluctuations in comparison with the other target AAILs and follows a relatively uniform distribution in the *x* direction because of its significant interaction with CO_2 gas. The presence of peaks at the same distances from each other, see Fig. 4c, in $[P_{4444}COOH][Gly]$ AAIL confirms that the gas has dissolved and the physical absorption process of the gas has occurred. Since the interaction of the anion with the gas is the strongest, the gas is expected to be observed wherever the anion is present; therefore, five different peaks are seen in the gas concentration profile which is a sign of gas distribution inside the AAIL. A graphical representation of the last orientation of CO_2 into the AAIL is shown in Fig. 5 which confirms the above discussion. As Fig. 5 shows, all studied AAILs can spread CO_2 gas inside free spaces of green solvent and in the case of $[P_{4444}COOH][Gly]$ AAIL, the gas is surrounded by anions. Considering other AAILs, it can be found that the distribution of anion around the cation or its accumulation without the presence of gas can also be seen in some areas of the simulation cell.

The squared displacement $|r_i(t) - r_i(0)|^2$ of *N* molecules in the simulation is used to determine the MSD at a time, *t*, of the simulated system. MSD is defined as [13,82]:

$$MSD_i(t) = \left\langle |r_i(t) - r_i(0)|^2 \right\rangle = \frac{1}{N}\sum_{i=1}^{N} |r_i(t) - r_i(0)|^2 \quad (2)$$

where *N* and $|r_i(t) - r_i(0)|$ stand for the particle number and the dislocation of the i^{th} particle at the running *t*, respectively. Fig. 6 shows the variation of MSD of the center of mass of AAIL ion pairs with a functional group in the alkyl cation chain at the final 1 ns of MD simulation. MSD value for functionalized AAIL with carboxylic acid group indicates the lowest mobility and AAIL containing methoxy group has the highest mobility in accordance to the computed AIQM results. The reason for this change in MSD values is that the size of the anion is smaller than the cation; in other words, the cation is bulkier than the anion and the anion is more mobile. Due to the lowest mobility of $[P_{4444}COOH]^+$ and $[Gly]^-$, it is expected that the strongest interaction with CO_2 gas is also observed in $[P_{4444}COOH][Gly]$ AAIL.

The variation of MSD with time as an initial value is applied to determine not only the diffusivity parameter [83] or β exponent [66] but also the diffusion coefficient of the system; if $\beta = \frac{dlogMSD}{dlogt} = 1$, the system is in the diffusive regime and the MSD changes linearly with the simulation time; as a consequence, the diffusion coefficient can be calculated by Einstein's relation [84]. In cases where $\beta < 1$, MSD has a linear relationship with t^{α}. In most cases, α is a number smaller than one and equal to 0.5 and in such a situation, the system is in the sub-diffusive regime. In cases where $MSD \propto t^{\alpha}$ and $\beta > 1$, the system is in the

Table 6
Values of the total, free, and occupied volume in Å^3 for pure AAIL at 298 K.

AAIL	Total volume	Free volume	Occupied volume	Free volume fraction
$[P_{4444}][Gly]$	29,088.11	4283.55	24,804.56	0.15
$[P_{4444}NH_2][Gly]$	29,088.72	3399.88	25,688.84	0.12
$[P_{4444}COOH][Gly]$	30,612.30	4278.02	26,334.28	0.14
$[P_{4444}OH][Gly]$	28,899.02	3789.04	25,109.98	0.13
$[P_{4444}OCH_3][Gly]$	30,359.14	3784.81	26,574.33	0.12

Table 5
Values of diffusion coefficients (*D*) of cation, anion, and CO_2 gas ($D \times 10^{-12}$ m^2/s), R^2, standard error (SE) of estimation, and gas diffusivity parameter (β).

	Cation			Anion			CO_2			
AAILs	*D*	R^2	SE	*D*	R^2	SE	*D*	R^2	SE	β
$[P_{4444}][Gly]$	7.22	0.96	0.24	5.14	0.93	0.23	41.88	0.58	5.83	0.47
$[P_{4444}NH_2][Gly]$	4.98	0.97	0.14	5.96	0.98	0.15	74.41	0.97	2.24	0.69
$[P_{4444}COOH][Gly]$	1.75	0.98	0.09	1.62	0.74	0.16	9.67	0.77	0.86	0.24
$[P_{4444}OH][Gly]$	3.94	0.91	0.09	2.77	0.80	0.23	17.76	0.91	0.93	0.50
$[P_{4444}OCH_3][Gly]$	9.53	0.99	0.13	10.49	0.99	0.16	68.13	0.98	1.76	0.68

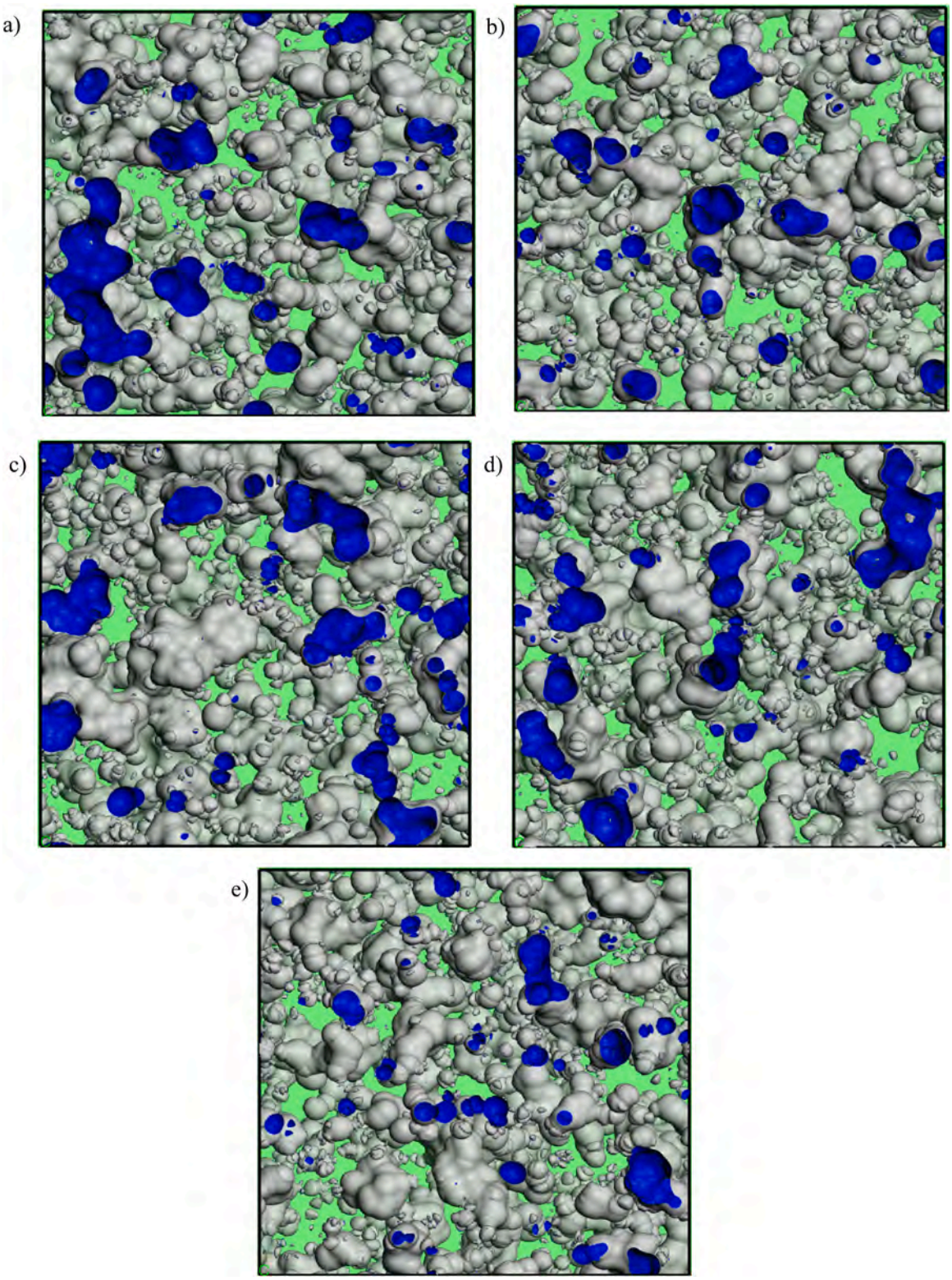

Fig. 7. Free volume of pure AAILs at 298 K a) [P_{4444}][Gly], b) [$P_{4444}NH_2$][Gly], c) [$P_{4444}COOH$][Gly], d) [$P_{4444}OH$][Gly] and e) [$P_{4444}OCH_3$][Gly]. The gray color shows the occupied volume and blue color shows the free volume.

super-diffusive regime. The self-diffusion coefficient is determined based on the MSD of each ion in the diffusive regime using Einstein's equation [13,85].

$$D = \lim_{t\to\infty} \frac{1}{6} \frac{dMSD}{dt} \tag{3}$$

The values of the diffusion coefficients of the center of mass of cation, anion, and CO_2 gas were computed by using the MD simulations at the production stage of MD, i.e., performing the simulation in the NVE ensemble by finding the slope of the MSD straight line against simulation time. Noticeably, the values of cation and anion self-diffusion coefficient values at pure [P_{4444}][Gly] AAIL are in good agreement with

Shaikh et al. [14] simulation results at 300 K by GAFF. The value of R^2, which measures the closeness to a straight line, is also reported in Table 5 along with the diffusion coefficient values and the standard error of the fitting.

As it is clear from Table 5, the values of cation and anion diffusion coefficients depend on the cation functionality and [P_{4444}COOH][Gly] has the lowest diffusion coefficient. In all cases, R^2 is greater than 0.91 and the standard error of estimation is very low. These both confirm the diffusive regime of mobility, i.e., a β value of 1. Nevertheless, the anion of [P_{4444}COOH][Gly] AAIL, as well as the gas diffusivity, do not follow the Fickian diffusivity that is related to gas capturing by AAIL; in other words, [P_{4444}COOH][Gly] can enjoy the greatest solubility of the gas. The values of dissolved gas β in all studied AAILs are less than one that reveals the behavior of gas is a sub-diffusive behavior; therefore, the diffusion of gas inside the AAIL is not completely uniform, i.e., a physical absorption has occurred. It can be seen that the largest deviation from one for β parameter is observed in [P_{4444}COOH][Gly] AAIL, which is due to the greater dissolution of the gas in the above-mentioned AAIL.

Free volume acts as a channel path for gas molecules to pass through the AAIL; it is placed where atoms are not present and there is a space between species of the system. The free volume is obtained using the Connolly surface. Atoms are represented by hard spheres with specific van der Waals radii. The Connolly surface is calculated when the probe molecule rotates on the van der Waals surface, and free volume is defined as the volume on the Connolly surface without atoms [86]. The free volume includes a volume that is not accessible to probe. The free volume and the occupied volume were calculated directly with the help of Materials Studio software and using the atom volumes and surfaces tool Module. The free volume values for all types of pure goal AAILs are reported in Table 6.

Even though numerically, the highest free volume is related to [P_{4444}][Gly] AAIL and after that, it is related to [P_{4444}COOH][Gly] AAIL, as the graphic representation of free volume (Fig. 7) shows, the free volumes in [P_{4444}][Gly] AAIL are isolated islands that are far from each other. From the other side of view, [P_{4444}COOH][Gly] AAIL contains continuous free channels that allow the gas molecules to pass through the AAIL. The amount of free and occupied volumes demonstrates if the AAIL has continuous free channels. The occupied volume at the presence of CO_2 gas is 25,308.69 $Å^3$ for a system containing [P_{4444}][Gly]+CO_2 at 298 K while it is 27,089.91 $Å^3$ for a system containing [$P_{4444}OCH_3$][Gly]+CO_2 at the same condition that is the lowest variation in occupied volume through gas capturing.

4. Conclusions

Phosphonium-based AAILs with glycinate as counter ion were considered for CO_2 gas trapping. The cation was functionalized by different functional groups and by MD simulation the effect of cation functionalization on CO_2 gas absorption was investigated for the first time as the authors are aware. AAIL with a carboxylic functional group ([P_{4444}COOH][Gly]) has the highest density and absorption energy as cation-anion interaction is the least. In addition, the volume difference between pure AAIL and its mixture state is the lowest one which indicates carbon dioxide gas interacts strongly with the above-mentioned AAIL. The trend of anion-cation, cation-CO_2, and anion-CO_2 pair correlation functions reveals that the strongest interaction between ion pair of AAIL inhibits the considerable interaction between AAIL and CO_2, as a result, CO_2 gas absorption occurs through anion species with an absorption energy of -1.917 kcal.mol^{-1}. Gas-anion pair distribution function in accordance with the absorption energy is the most significant one in [P_{4444}COOH][Gly] AAIL. Moreover, the anion-gas coordination number displays that each ion pair has a capacity of 2 CO_2 molecules to be absorbed. Not only does the gas concentration profile exhibit that [P_{4444}COOH][Gly] AAIL enjoys gas solubility but also both cation and anion have the lowest mobility values due to the interaction with the captured gas. The free volume for [P_{4444}COOH][Gly] AAIL is considerable as well as constructing continuous channels that lead to the possibility of gas considerable absorption. Finally, it can be summarized that withdrawing functional groups in cation structure improves CO_2 gas absorption capacity.

Declaration of Competing Interest

The authors declare the following financial interests/personal relationships which may be considered as potential competing interests: Fatemeh Moosavi reports financial support was provided by Ferdowsi University of Mashhad. Fatemeh Moosavi reports a relationship with Ferdowsi University of Mashhad that includes: employment.

Acknowledgments

This research project was financially supported by Ferdowsi University of Mashhad, Iran (grant No. 3/55635). The computations were partly carried out in the High-Performance Computing (HPC) Center at Ferdowsi University of Mashhad. The authors would like to appreciate Ferdowsi Cloud cooperation.

References

[1] J.D. Figueroa, T. Fout, S. Plasynski, H. Mcilvried, R.D. Srivastava, Advances in CO_2 capture technology—the U.S. department of energy's carbon sequestration program, Int. J. Greenh. Gas. Control 2 (2008) 9–20.
[2] N. Noorani, A. Mehrdad, I. Ahadzadeh, CO_2 absorption in amino acid-based ionic liquids: experimental and theoretical studies, Fluid Phase Equilibria 547 (2021), 113185.
[3] H. Harde, Scrutinizing the carbon cycle and CO_2 residence time in the atmosphere, Glob. Planet. Change 152 (2017) 19–26.
[4] X. Luo, C. Wang, The development of carbon capture by functionalized ionic liquids. Current opinion in green and sustainable, Chemistry 3 (2017) 33–38.
[5] K. Anderson, M.P. Atkins, J. Estager, Y. Kuah, S. Ng, A.A. Oliferenko, N. V. Plechkova, A.V. Puga, K.R. Seddon, D.F. Wassell, Carbon dioxide uptake from natural gas by binary ionic liquid–water mixtures, Green. Chem. 17 (2015) 4340–4354.
[6] Z. Tian, S. Dai, D.-E. Jiang, What can molecular simulation do for global warming? WIREs Comput. Mol. Sci. 6 (2016) 173–197.
[7] J.G. Neumann, H. Stassen, Anion effect on gas absorption in imidazolium-based ionic liquids, J. Chem. Inf. Model. 60 (2020) 661–666.
[8] V.V. Chaban, Carbon dioxide chemisorption by ammonium and phosphonium ionic liquids: quantum chemistry calculations, J. Phys. Chem. B 126 (2022) 5497–5506.
[9] F.A. Rahman, M.M.A. Aziz, R. Saidur, Bakar Wawa, M.R. Hainin, R. Putrajaya, N. A. Hassan, Pollution to solution: capture and sequestration of carbon dioxide (CO_2) and its utilization as a renewable energy source for a sustainable future, Renew. Sustain. Energy Rev. 71 (2017) 112–126.
[10] K.M.K. Yu, I. Curcic, J. Gabriel, S.C.E. Tsang, Recent Advances in CO_2 Capture and Utilization, ChemSusChem 1 (2008) 893–899.
[11] M. Wang, A. Lawal, P. Stephenson, J. Sidders, C. Ramshaw, Post-combustion CO_2 capture with chemical absorption: a state-of-the-art review, Chem. Eng. Res. Des. 89 (2011) 1609–1624.
[12] Q.R. Sheridan, W.F. Schneider, E.J. Maginn, Role of molecular modeling in the development of CO_2-reactive ionic liquids, Chem. Rev. 118 (2018) 5242–5260.
[13] J. Tong, Y. Zhao, F. Huo, Y. Guo, X. Liang, N. Von Solms, H. He, The dynamic behavior and intrinsic mechanism of CO_2 absorption by amino acid ionic liquids, Phys. Chem. Chem. Phys. 23 (2021) 3246–3255.
[14] A.R. Shaikh, M. Ashraf, T. Almayef, M. Chawla, A. Poater, L. Cavallo, Amino acid ionic liquids as potential candidates for CO_2 capture: Combined density functional theory and molecular dynamics simulations, Chem. Phys. Lett. 745 (2020), 137239.
[15] J.-H. Yim, W.-W. Seo, J.S. Lim, CO_2 Solubility in Bis(trifluoromethylsulfonyl)imide ([Tf_2N]) Anion-Based Ionic Liquids: [BVIM][Tf_2N], [P_{4441}][Tf_2N], and [N_{4222}][Tf_2N], J. Chem. Eng. Data 67 (2021) 3–13.
[16] Y. Qu, Y. Zhao, D. Li, J. Sun, Task-specific ionic liquids for carbon dioxide absorption and conversion into value-added products. Current Opinion in Green and Sustainable, Chemistry 34 (2022), 100599.
[17] T. Ma, J. Wang, Z. Du, A.A. Abdeltawab, A.M. Al-Enizi, X. Chen, G. Yu, A process simulation study of CO_2 capture by ionic liquids, Int. J. Greenh. Gas. Control 58 (2017) 223–231.
[18] M. Aghaie, N. Rezaei, S. Zendehboudi, A systematic review on CO_2 capture with ionic liquids: current status and future prospects, Renew. Sustain. Energy Rev. 96 (2018) 502–525.
[19] Q. Sohaib, M.A. Kazemi, C. Charmette, J. Cartier, M. Younas, A. Azarafza, M. Rezakazemi, J. Sanchez-Marcano, CO_2 solubility and diffusivity in 1-ethyl-3-methylimidazolium cation-based ionic liquids; isochoric pressure drop approach, Fluid Phase Equilibria 563 (2022), 113581.
[20] M. Królikowski, M. Więckowski, M. Ebrahiminejadhasanabadi, W.M. Nelson, P. Naidoo, D. Ramjugernath, U. Domańska, Carbon dioxide solubility in ionic

liquids: [Guad-(6,6),(1,1),(1,1)][DCA] and [Guad-(6,6),(1,1),(1,1)][TCM] at high pressure, Fluid Phase Equilibria 563 (2022), 113572.
[21] E. Torralba-Calleja, J. Skinner, D. Gutiérrez-Tauste, CO_2 capture in ionic liquids: a review of solubilities and experimental methods, J. Chem. 2013 (2013), 473584.
[22] L. Zhou, J. Fan, X. Shang, CO_2 capture and separation properties in the ionic liquid 1-n-butyl-3-methylimidazolium nonafluorobutylsulfonate, Materials 7 (2014) 3867–3880.
[23] Y. Xie, G. Liu, H. Nie, F. Yu, X. Xing, H. Cui, Energy analysis of physical absorption and chemical absorption of CO_2 in ionic liquids. energy, Technology (2019) 8.
[24] Y.S. Sistla, L. Jain, A. Khanna, Validation and prediction of solubility parameters of ionic liquids for CO_2 capture, Sep. Purif. Technol. 97 (2012) 51–64.
[25] Kuroki N., Suzuki Y., Kodama D., Chowdhury F.A., Yamada H, and H.M. Ultrafast Realization of Ionic Liquids with Excellent CO2 Absorption: A trinity study of machine learning, synthesis, and precision measurement. Cambridge: Cambridge Open Engage. 2022.
[26] R.L. Gardas, R. Ge, P. Goodrich, C. Hardacre, A. Hussain, D.W. Rooney, Thermophysical properties of amino acid-based ionic liquids, J. Chem. Eng. Data 55 (2010) 1505–1515.
[27] P.J. Carvalho, V.H. Álvarez, I.M. Marrucho, M. Aznar, J.A.P. Coutinho, High carbon dioxide solubilities in trihexyltetradecylphosphonium-based ionic liquids, J. Supercrit. Fluids 52 (2010) 258–265.
[28] M. Rezaeian, M. Izadyar, Nakhaei, Pour A. carbon dioxide absorption by the imidazolium–amino acid ionic liquids, kinetics, and mechanism approach, J. Phys. Chem. A 122 (2018) 5721–5729.
[29] O. Hollóczki, Z. Kelemen, L. Könczöl, D. Szieberth, L. Nyulászi, A. Stark, B. Kirchner, Significant cation effects in carbon dioxide–ionic liquid systems, ChemPhysChem 14 (2013) 315.
[30] J.L. Anthony, E.J. Maginn, J.F. Brennecke, Solubilities and thermodynamic properties of gases in the ionic liquid 1-n-Butyl-3-methylimidazolium hexafluorophosphate, J. Phys. Chem. B 106 (2002) 7315–7320.
[31] S. Hanioka, T. Maruyama, T. Sotani, M. Teramoto, H. Matsuyama, K. Nakashima, M. Hanaki, F. Kubota, M. Goto, CO_2 separation facilitated by task-specific ionic liquids using a supported liquid membrane, J. Membr. Sci. 314 (2008) 1–4.
[32] X.-Y. Luo, X.-Y. Chen, R.-X. Qiu, B.-Y. Pei, Y. Wei, M. Hu, J.-Q. Lin, J.-Y. Zhang, G.-G. Luo, Enhanced CO_2 capture by reducing cation–anion interactions in hydroxyl-pyridine anion-based ionic liquids, Dalton Trans. 48 (2019) 2300–2307.
[33] S. Khazalpour, M. Yarie, E. Kianpour, A. Amani, S. Asadabadi, J.Y. Seyf, M. Rezaeivala, S. Azizian, M.A. Zolfigol, Applications of phosphonium-based ionic liquids in chemical processes, J. Iran. Chem. Soc. 17 (2020) 1775–1917.
[34] C.J. Bradaric, A. Downard, C. Kennedy, A.J. Robertson, Y. Zhou, Industrial preparation of phosphonium ionic liquids, Green. Chem. 5 (2003) 143–152.
[35] F.-F. Chen, K. Huang, J.-P. Fan, D.-J. Tao, Chemical solvent in chemical solvent: a class of hybrid materials for effective capture of CO_2, AIChE J. 64 (632–639) (2018).
[36] S. Kasahara, E. Kamio, A.R. Shaikh, T. Matsuki, H. Matsuyama, Effect of the amino-group densities of functionalized ionic liquids on the facilitated transport properties for CO_2 separation, J. Membr. Sci. 503 (2016) 148–157.
[37] D.S. Firaha, B. Kirchner, Tuning the carbon dioxide absorption in amino acid ionic liquids, ChemSusChem 9 (2016) 1591–1599.
[38] Y.S. Sistla, A. Khanna, CO_2 absorption studies in amino acid-anion based ionic liquids, Chem. Eng. J. 273 (2015) 268–276.
[39] P. Prakash, A. Venkatnathan, Molecular mechanism of CO_2 absorption in phosphonium amino acid ionic liquid, RSC Adv. 6 (2016) 55438–55443.
[40] K. Fukumoto, M. Yoshizawa, H. Ohno, Room temperature ionic liquids from 20 natural amino acids, J. Am. Chem. Soc. 127 (2005) 2398–2399.
[41] J. Zhang, S. Zhang, K. Dong, Y. Zhang, Y. Shen, X. Lv, Supported absorption of CO_2 by tetrabutylphosphonium amino acid ionic liquids, Chem. – A Eur. J. 12 (2006) 4021–4026.
[42] S. Kasahara, E. Kamio, T. Ishigami, H. Matsuyama, Effect of water in ionic liquids on CO_2 permeability in amino acid ionic liquid-based facilitated transport membranes, J. Membr. Sci. 415–416 (2012) 168–175.
[43] D. Hospital-Benito, J. Lemus, C. Moya, R. Santiago, J. Palomar, Process analysis overview of ionic liquids on CO_2 chemical capture, Chem. Eng. J. 390 (2020), 124509.
[44] Q.R. Sheridan, S. Oh, O. Morales-Collazo, E.W. Castner, J.F. Brennecke, E. J. Maginn, Liquid structure of CO_2–reactive aprotic heterocyclic anion ionic liquids from x-ray scattering and molecular dynamics, J. Phys. Chem. B 120 (2016) 11951–11960.
[45] X.Y. Luo, X. Fan, G.L. Shi, H.R. Li, C.M. Wang, Decreasing the viscosity in CO_2 capture by amino-functionalized ionic liquids through the formation of intramolecular hydrogen bond, J. Phys. Chem. B 120 (2016) 2807–2813.
[46] Y. Chen, F. Mutelet, J.-N. Jaubert, Modeling the solubility of carbon dioxide in imidazolium-based ionic liquids with the PC-SAFT equation of state, J. Phys. Chem. B 116 (2012) 14375–14388.
[47] C. Panayiotou, V. Hatzimanikatis, The solubility parameters of carbon dioxide and ionic liquids: are they an enigma? Fluid Phase Equilibria 527 (2021), 112828.
[48] A. Li, Z. Tian, T. Yan, D.-E. Jiang, S. Dai, Anion-functionalized task-specific ionic liquids: molecular origin of change in viscosity upon CO_2 capture. The, J. Phys. Chem. B 118 (2014) 14880–14887.
[49] S. Kang, Y.G. Chung, J.H. Kang, H. Song, CO_2 absorption characteristics of amino group functionalized imidazolium-based amino acid ionic liquids, J. Mol. Liq. 297 (2020), 111825.
[50] Y. Zhang, S. Zhang, X. Lu, Q. Zhou, W. Fan, X. Zhang, Dual amino-functionalised phosphonium ionic liquids for CO_2 capture, Chem. Eur. J. 15 (2009) 3003–3011.
[51] A.R. Shaikh, H. Karkhanechi, E. Kamio, T. Yoshioka, H. Matsuyama, Quantum mechanical and molecular dynamics simulations of dual-amino-acid ionic liquids for CO_2 capture, J. Phys. Chem. C. 120 (2016) 27734–27745.
[52] D. Zhao, Y. Liao, Z. Zhang, Toxicity of ionic liquids, CLEAN – Soil, Air, Water 35 (2007) 42–48.
[53] T. Liu, P. Panwar, A. Khajeh, M.H. Rahman, P.L. Menezes, A. Martini, Review of molecular dynamics simulations of phosphonium ionic liquid lubricants, Tribology Lett. 70 (2022) 44.
[54] Frisch M.J., Trucks G.W., Schlegel H.B., Scuseria G.E., Robb M.A., Cheeseman J.R., Scalmani G., Barone V., Mennucci B., Petersson G.A., Nakatsuji H., Caricato M., Li X., Hratchian H.P., Izmaylov A.F., Bloino J., Zheng G., Sonnenberg J.L., Hada M., Ehara M., Toyota K., Fukuda R., Hasegawa J., Ishida M., Nakajima T., Honda Y., Kitao O., Nakai H., Vreven T., Montgomery J., J.A., Peralta J.E., Ogliaro F., Bearpark M.J., Heyd J.J., Brothers E.N., Kudin K.N., Staroverov V.N., Kobayashi R., Normand J., Raghavachari K., Rendell A.P., Burant J.C., Iyengar S.S., Tomasi J., Cossi M., Rega N., Millam J.M., Klene M., Knox J.E., Cross J.B., Bakken V., Adamo C., Jaramillo J., Gomperts R., Stratmann R.E., Yazyev O., Austin A.J., Cammi R., Pomelli C., Ochterski J.W., Martin R.L., Morokuma K., Zakrzewski V.G., Voth G.A., Salvador P., Dannenberg J.J., Dapprich S., Daniels A.D., Farkas O., Foresman J.B., Ortiz J.V., Cioslowski J, and Fox D.J., Gaussian 09, Revision A.01. 2009.
[55] M. Meunier, S. Robertson, Materials Studio 20th anniversary, Mol. Simul. 47 (2021) 537–539.
[56] M. Meunier, Guest Editorial, Mol. Simul. 34 (2008) 887–888.
[57] H. Sun, COMPASS: an ab initio force-field optimized for condensed-phase applications-overview with details on alkane and benzene compounds, J. Phys. Chem. B 102 (1998) 7338–7364.
[58] B. Derecskei, A. Derecskei-Kovacs, Molecular modelling simulations to predict density and solubility parameters of ionic liquids, Mol. Simul. 34 (2008) 1167–1175.
[59] E. Weinan, D. Li, The Andersen thermostat in molecular dynamics, Commun. pure Appl. Math. 61 (2008) 96–136.
[60] H.J.C. Berendsen, J.P.M. Postma, W.F. Van Gunsteren, A. Dinola, J.R. Haak, Molecular dynamics with coupling to an external bath, J. Chem. Phys. 81 (1984) 3684–3690.
[61] M. Razmkhah, Effects of carboxylic group on bulk and electrical double layer properties of amino acid ionic liquid, J. Mol. Liq. 299 (2020), 112158.
[62] M.H. Ghatee, A.R. Zolghadr, F. Moosavi, Y. Ansari, Studies of structural, dynamical, and interfacial properties of 1-alkyl-3-methylimidazolium iodide ionic liquids by molecular dynamics simulation, J. Chem. Phys. (2012) 136.
[63] M.H. Kowsari, S. Alavi, M. Ashrafizaadeh, B. Najafi, Molecular dynamics simulation of imidazolium-based ionic liquids. II. Transport coefficients, J. Chem. Phys. (2009) 130.
[64] M.H. Kowsari, S. Alavi, B. Najafi, K. Gholizadeh, E. Dehghanpisheh, F. Ranjbar, Molecular dynamics simulations of the structure and transport properties of tetra-butylphosphonium amino acid ionic liquids, Phys. Chem. Chem. Phys. 13 (2011) 8826–8837.
[65] X. Liu, Y. Zhao, X. Zhang, G. Zhou, S. Zhang, Microstructures and interaction analyses of phosphonium-based ionic liquids: a simulation study, J. Phys. Chem. B 116 (2012) 4934–4942.
[66] M.H. Kowsari, S. Alavi, M. Ashrafizaadeh, B. Najafi, Molecular dynamics simulation of imidazolium-based ionic liquids. I. Dynamics and diffusion coefficient. The, J. Chem. Phys. 129 (2008), 224508.
[67] A.R. Zolghadr, M.H. Ghatee, F. Moosavi, The effect of various quantum mechanically derived partial atomic charges on the bulk properties of chloride-based ionic liquids, Chem. Phys. 475 (2016) 23–31.
[68] X. Liu, G. Zhou, S. Zhang, G. Yu, Molecular simulations of phosphonium-based ionic liquid, Mol. Simul. 36 (2010) 79–86.
[69] Y. Zhao, L. Tian, Y. Pei, H. Wang, J. Wang, Effect of anionic structure on the LCST phase behavior of phosphonium ionic liquids in water, Ind. Eng. Chem. Res. 57 (2018) 12935–12941.
[70] G. Zhou, X. Liu, S. Zhang, G. Yu, H. He, A force field for molecular simulation of tetrabutylphosphonium amino acid ionic liquids, J. Phys. Chem. B 111 (2007) 7078–7084.
[71] C. Jin, M. Chen, M. Fan, G. Luo, M. Shao, Z. Huang, X. Xie, Hydrophobic phosphonium-based ionic liquids as novel extractants for palladium(II) recovery from alkaline cyanide solutions, J. Mol. Liq. 336 (2021), 116358.
[72] C. Jiang, S. Zeng, X. Ma, J. Feng, G. Li, L. Bai, F. Li, X. Ji, X. Zhang, Aprotic phosphonium-based ionic liquid as electrolyte for high CO_2 electroreduction to oxalate, AIChE J. 69 (2023), e17859.
[73] D. Thompson, S. Coleman, D. Diamond, R. Byrne, Electronic structure calculations and physicochemical experiments quantify the competitive liquid ion association and probe stabilisation effects for nitrobenzospiropyran in phosphonium-based ionic liquids, Phys. Chem. Chem. Phys. 13 (2011) 6156–6168.
[74] S. Saravanamurugan, A.J. Kunov-Kruse, R. Fehrmann, A. Riisager, Amine-functionalized amino acid-based ionic liquids as efficient and high-capacity absorbents for CO_2, ChemSusChem 7 (2014) 897–CO902.
[75] Y.-L. Wang, F.U. Shah, S. Glavatskih, O.N. Antzutkin, A. Laaksonen, Atomistic insight into orthoborate-based ionic liquids: force field development and evaluation, J. Phys. Chem. B 118 (2014) 8711–8723.
[76] B.E. Gurkan, J.C. De La Fuente, E.M. Mindrup, L.E. Ficke, B.F. Goodrich, E.A. Price, W.F. Schneider, J.F. Brennecke, Equimolar CO_2 Absorption by Anion-Functionalized Ionic Liquids, J. Am. Chem. Soc. 132 (2010) 2116–2117.
[77] T.B. Lee, S. Oh, T.R. Gohndrone, O. Morales-Collazo, S. Seo, J.F. Brennecke, W. F. Schneider, CO_2 chemistry of phenolate-based ionic liquids, J. Phys. Chem. B 120 (2016) 1509–1517.

[78] J.N. Canongia Lopes, A.A.H. Pádua, Molecular force field for ionic liquids iii: imidazolium, pyridinium, and phosphonium cations; chloride, bromide, and dicyanamide anions, J. Phys. Chem. B 110 (2006) 19586–19592.
[79] B. Zhang, A.C.T. Van Duin, J.K. Johnson, Development of a ReaxFF reactive force field for tetrabutylphosphonium glycinate/CO_2 mixtures, J. Phys. Chem. B 118 (2014) 12008–12016.
[80] Q. Yang, Z. Wang, Z. Bao, Z. Zhang, Y. Yang, Q. Ren, H. Xing, S. Dai, New Insights into CO_2 absorption mechanisms with amino-acid ionic liquids, ChemSusChem 9 (2016) 806–812.
[81] H. Nadimi, M.R. Housaindokht, F. Moosavi, The effect of anion on aggregation of amino acid ionic liquid: atomistic simulation, J. Mol. Graph. Model. 101 (2020), 107733.
[82] Alavi S., Molecular simulations: fundamentals and practice. 2020: John Wiley & Sons.
[83] U.A. Higgoda, R. Hellmann, T.M. Koller, A.P. Fröba, Self-diffusion coefficient and viscosity of methane and carbon dioxide via molecular dynamics simulations based on new ab initio-derived force fields, Fluid Phase Equilibria 481 (2019) 15–27.
[84] L. You, Y. Guo, Y. He, F. Huo, S. Zeng, C. Li, X. Zhang, X. Zhang, Molecular level understanding of CO_2 capture in ionic liquid/polyimide composite membrane, Front. Chem. Sci. Eng. 16 (2022) 141–151.
[85] A.R. Shaikh, E. Kamio, H. Takaba, H. Matsuyama, Effects of water concentration on the free volume of amino acid ionic liquids investigated by molecular dynamics simulations, J. Phys. Chem. B 119 (2015) 263–273.
[86] H. Riasat Harami, F. Amirkhani, S.A. Khadem, M. Rezakazemi, M. Asghari, S. Shirazian, Mass transfer through PDMS/zeolite 4A MMMs for hydrogen separation: molecular dynamics and grand canonical Monte Carlo simulations, Int. Commun. Heat. Mass Transf. 108 (2019), 104259.